Journal of proteome research

Article

pubs.acs.org/jpr

Imaging Mass Spectrometry for Assessing Cutaneous Wound Healing: Analysis of Pressure Ulcers

Domenico Taverna,[†] Alonda C. Pollins,[‡] Giovanni Sindona,[§] Richard M. Caprioli,[∥] and Lillian B. Nanney*[,⊥]

[†]Dipartimento di Chimica e Tecnologie Chimiche, Università della Calabria, Via P. Bucci, cubo 12/D, Arcavacata di Rende, CS, 87036, Italy

[‡]Vanderbilt University Medical Center, 1161 21st Avenue South, MCN S2221, Nashville, Tennessee 37232-2631, United States

[§]Dipartimento di Chimica e Tecnologie Chimiche, Università della Calabria, Via P. Bucci, cubo 12/C, Arcavacata di Rende, CS, 87036, Italy

[∥]Mass Spectrometry Research Center, Departments of Chemistry, Pharmacology, and Biochemistry, Vanderbilt University School of Medicine, 465 21st Avenue South, Medical Research Building 3, Room 9160, Nashville, Tennessee 37232-8575, United States

[⊥]Plastic Surgery Research Laboratory, Vanderbilt University School of Medicine 1161 21st Avenue South, MCN S2221, Nashville, Tennessee 37232-2631, United States

Supporting Information

ABSTRACT: Imaging mass spectrometry (IMS) was employed for the analysis of frozen skin biopsies to investigate the differences between stage IV pressure ulcers that remain stalled, stagnant, and unhealed versus those exhibiting clinical and histological signs of improvement. Our data reveal a rich diversity of proteins that are dynamically modulated, and we selectively highlight a family of calcium binding proteins (S-100 molecules) including calcyclin (S100-A6), calgranulins A (S100-A8) and B (S100-A9), and calgizzarin (S100-A11). IMS allowed us to target three discrete regions of interest: the wound bed, adjacent dermis, and hypertrophic epidermis. Plots derived using unsupervised principal component analysis of the global protein signatures within these three spatial niches indicate that these data from wound signatures have potential as a prognostic tool since they appear to delineate wounds that are favorably responding to therapeutic interventions versus those that remain stagnant or intractable in their healing status. Our discovery-based approach with IMS augments current knowledge of the molecular signatures within pressure ulcers while providing a rationale for a focused examination of the role of calcium modulators within the context of impaired wound healing.

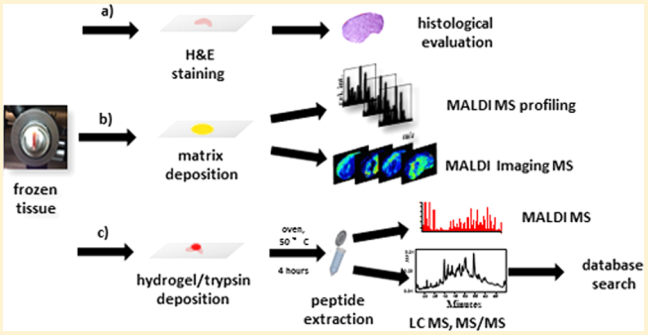

KEYWORDS: *Pressure ulcers, imaging mass spectrometry, S-100 proteins, chronic wounds, proteomics, human defensin 6, calgranulin A, calgranulin B, calgizzarin, calcyclin*

INTRODUCTION

Experimental procedures for large-scale global proteome analyses typically examine differential expression of hundreds of proteins between two or more biological states. In many cases, these proteins become potential biomarker candidates, and a select few may eventually move through the development pathway to become therapeutic targets. Proteomics is fundamentally reliant on the power of mass spectrometry (MS) for rapid and specific protein analysis. Mass spectrometric methodologies provide a rapid and sensitive tool for identification and quantitation of analytes[1,2] as well as for direct analysis of protein mixtures, with less emphasis on preliminary protein purification steps.[3,4] A subset within this field of study is MALDI imaging MS (MALDI IMS),[5] a consolidated tool for the analysis of biological and clinical tissue samples[6] that has become an enabling technology in biological and medical research fields.[7−10] Applications of MALDI IMS include analysis of proteins,[11−13] peptides (both endogenous and enzymatically produced),[14−17] lipids,[18−20] drugs and metabolites,[21,22] and oligonucleotides.[23] Endogenous as well as exogenous molecules can be analyzed directly from the tissue in their native environment, providing new insights into the biological process involved. Direct analysis on intact tissue preserves the spatial relationship of molecules within a specimen while requiring minimal sample preparation. Thin tissue sections (typically, 5−12 μm thick) are obtained from fresh frozen or formalin-fixed paraffin-embedded (FFPE) tissues and collected onto conductive targets. A matrix compound (typically, a small organic acid as well as a

Received: September 30, 2014
Published: December 8, 2014

   dx.doi.org/10.1021/pr5010218 | J. Proteome Res. 2015, 14, 986−996

proteolytic enzyme when necessary) is deposited onto the surface of a tissue sample in one of a few different ways (e.g., by spotting, subliming, or spraying). The target is analyzed by the mass spectrometer. Mass spectra are subsequently produced through laser ablation of a multitude of spots or pixels located on the sample. Intensity plots, or images, are constructed for each m/z value by plotting intensities in two-dimensional spaces, resulting in hundreds of images (ion density maps) being recorded in a single MALDI IMS experiment.

The present study was designed to inform the field of impaired wound healing, where molecular mechanisms are poorly defined, through the utilization of the enabling technology of MALDI IMS as a discovery tool. Among the three major categories of chronic wounds, pressure ulcers were selected for analysis since this type of ulcer has recently come under closer scrutiny as an indicator of quality control in acute and long-term care facilities as reimbursement rules have become more stringent for those patients who acquire an ulcer during their hospital stay. The current economic climate thus offers a strong impetus to reduce the occurrence of pressure ulcers, to better understand the molecular disturbances in the wounds, and then to design more effective treatments. Clearly, a diagnostic tool and better understanding of the molecular disturbances within a wound bed would advance the field.

A pressure ulcer is a localized injury to the skin and underlying tissue usually over a bony prominence as a result of pressure or pressure in combination with shear and friction.[24] In current clinical practice, modern prognostic tools have not been applied to this disease. Bedside assessment of pressure ulcers is based on categorization into six visual stages, and accurate staging is wholly dependent on the experience of the healthcare provider.[25] The clinical determination of whether a wound is responding to the treatment of choice is based solely on subjective visual appearance of the wound, as objective measures have not been established. While a number of contributing or confounding factors, such as pre-existing medical conditions and socio-economic factors, are strongly associated with pressure ulcers, the significance of these factors in the development of a pressure ulcer is yet to be elucidated.[26,27]

In recognition that millions of patients on a worldwide basis are afflicted with chronic wounds that impose physical, psychosocial, and economic stresses to patients and burden society,[28] investigators have recently turned their attention toward elucidating proteomic changes occurring within pressure ulcers. The earliest proteomic reports analyzed wound fluids to provide the first glimpse of molecular events within chronic pressure ulcers.[29] In 2011, our group reported our initial studies using IMS to assess the distribution of proteins and lipids within skin ulcer tissue sections as compared to discrete areas within normal skin.[30,31]

The present IMS study was designed to extend our earlier proteomic findings using stage IV pressure ulcers. Although we report global proteomic disturbances, we selectively describe the spatial distribution of calcium binding proteins collected from ulcers displaying clinical evidence of continued chronicity in contrast to those showing clinical and morphologic evidence of healing. Some samples also displayed an intermediate stage of healing, depicting a possible shift in the wound response. Our study suggests that protein signatures may eventually serve as useful indicators to address whether chronic wounds remain stalled and stagnant or whether they are responding appropriately to therapeutic intervention and showing positive progression toward healing.

EXPERIMENTAL SECTION

Tissue Specimen Collection and Processing

Samples (n = 15) were obtained from patients on the Plastic Surgery Service undergoing surgical excision of large stage IV pressure ulcers prior to coverage with a local skin flap. To maintain a degree of standardization among these wound types, sample collection was restricted to the edge of the wound. The surgeon was queried for his subjective impressions as to whether that portion of the wound was showing evidence of improvement or was stagnant. Consent was obtained to use these discarded specimens for research purposes in accordance with Vanderbilt's Institutional Review Board. Samples were wrapped in aluminum foil, snap frozen in liquid nitrogen, and then stored at −80 °C. Adjacent companion samples for histological analysis were collected in 10% neutral buffered formalin (10% NBF), fixed for 24−48 h, and paraffin embedded.

Tissue Preparation and IMS Analysis

Frozen tissues were sectioned at 12 μm using a cryostat (CM3050 S, Leica Microsystems GmbH, Wetzlar, Germany) and fixed on ITO conductive glass slides while serial sections were collected on microscope slides for hematoxylin and eosin staining.[31] Tissue sections were gently washed prior to matrix deposition for MALDI analysis to remove salts, lipids, and general contaminants using a series of solutions (ethanol 70%, 30 s; ethanol 95%, 30 s; Carnoy's fluid, 120 s; ethanol 100%, 30 s; water, 30 s; ethanol 100%, 30 s) and were allowed to dry for 3 min at room temperature. For imaging experiments, sections were coated with a thin homogeneous layer of matrix using a sublimation device (Chemglass Life Science, Vineland, NJ, USA). Sublimation of sinapinic acid (300 mg) was carried out at 138 °C, at a pressure of 50 mTorr. After 17 min, ITO slides with the tissue on the upper surface became uniformly coated with a thin matrix layer. Finally, tissue sections were rehydrated at 85 °C for 3 min to allow matrix recrystallization. MS analysis were performed by a AutoflexSpeed MALDI TOF spectrometer (Bruker Daltonics, Billerica, MA, USA), equipped with a linear TOF analyzer, operating in positive polarity and accumulating 100 laser shots per position at 1000 Hz laser frequency over the m/z range of 2500−30 000. The laser intensity was adjusted before each experiment to yield optimal results. Images were acquired by a rastering pattern at 50 and 100 μm spatial resolution. Flex Control 3.3 software (Bruker Daltonics, Billerica, MA, USA) was used for spectra acquisition, and Flex Imaging 3.0, for image acquisition and ion density two-dimensional plots generation. Prior to generation of ion density maps, acquired spectra were normalized to the total ion current (TIC) in order to minimize spectrum-to-spectrum differences in peak intensity.

Statistical Analysis

Multiple spectra within the three regions of interest (wound bed, adjacent dermis, and hypertrophic epidermis at the wound margin) were selected from the MALDI IMS data. In particular, 200 spectra per area of interest were exported using the ion density maps of specific molecular features as coordinates. Comparisons of these regions of interest within different healing conditions were made using principal component analysis (PCA) based on protein profile patterns. These data

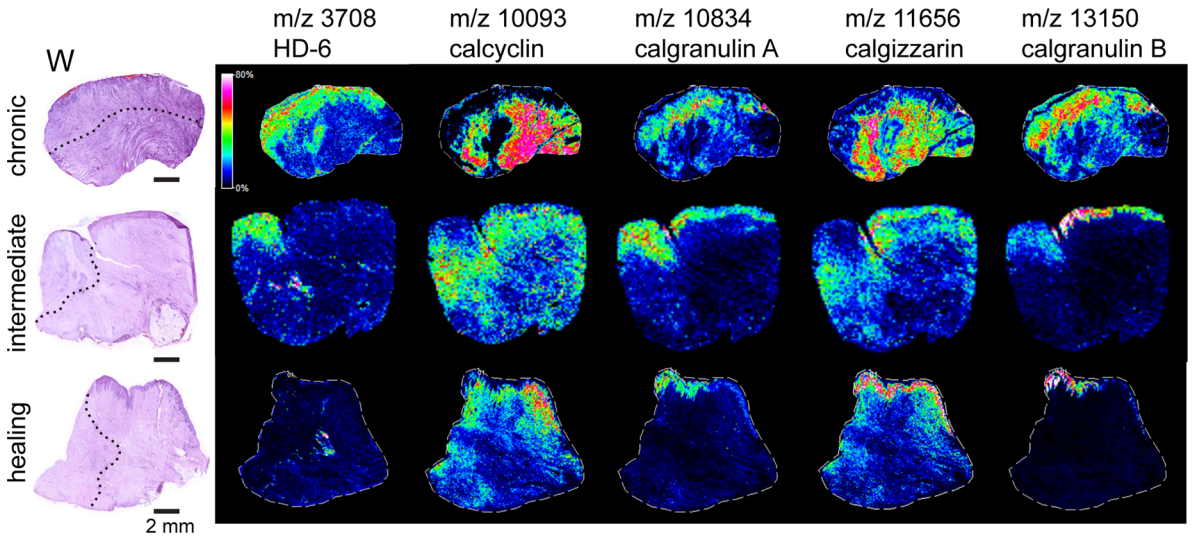

Figure 1. Two-dimensional ion density maps for human defensin 6 (HD-6) and 4 calcium related proteins: calcyclin, calgranulin A, calgizzarin, and calgranulin B. The left column (W) shows histological staining for three types of chronic pressure ulcers: a chronic (stagnating) example, a wound showing modest evidence of healing (intermediate along the healing continuum), and an ulcer that is definitely improving. Dotted lines divide the wound into focal regions of interest. Those above or to the left were sampled as wound bed, and areas to the right or below were sampled as nearby adjacent dermis. The color bar indicates the relative intensity of the particular ion, with red/pink colors representing the highest values and the blue/purple/black representing areas of low or nondetectable values.

were used to confirm the existence of three disparate regions within the wound tissues according to the protein pattern differences. Furthermore, data sets were processed using ClinProTools 2.2 software (Bruker Daltonics, Billerica, MA, USA): spectra were selected (100 maximal peak number, S/N threshold set at 5) and sorted by *p*-value (Wilcoxon/Kruskal–Wallis), and baselines were subtracted using Top Hat and recalibrated. PCA analyses were run after TIC spectra normalization.

In Situ Digestion, LC Analysis, and Protein ID

In situ digestion was carried out using spots of hydrogel (1 mm diameter) adapting a method described by Harris et al.[32,33] Briefly, hydrogels were rehydrated and expanded in 20 μL of 1 μg/mL trypsin (in 100 mM ammonium bicarbonate) and then placed on the tissue regions of interest according to the histology. The frozen sections, with hydrogels in place, were incubated at 50 °C, allowing digestion. After 4 h, hydrogels were removed from the tissue sections and collected individually. After the digestion, peptides were extracted by organic (50% acetonitrile/5% formic acid) and aqueous (100 mM ammonium bicarbonate) solvents (process repeated three times). The supernatants of each extraction were combined and dried in a centrifugal vacuum concentrator (SPD Speedvac, Thermo Scientific, Waltham, MA, USA). The reconstituted extracts (20 μL, 0.1% formic acid) were stored at −80 °C until LC–MS/MS analysis.

Resulting peptides were analyzed by a 70 min data-dependent LC–MS/MS analysis. Briefly, peptides were loaded via pressure cell onto a 40 mm × 0.1 mm self-packed reversed-phase (Jupiter 5 μm, 300A Phenomonex) trapping column fritted into an M520 filter union (IDEX). After loading and equilibration, this trapping column was attached to a 200 mm × 0.1 mm (Jupiter 3 μm, 300A), self-packed analytical column coupled directly to an LTQ (ThermoFisher, San Jose, CA, USA) using a nanoelectrospray source. A series of a full-scan mass spectrum followed by five data-dependent tandem mass spectra (MS/MS) were collected using the run-and-dynamic exclusion feature that was enabled to minimize acquisition of redundant spectra. MS/MS spectra were searched via SEQUEST against a human database (UniProtKB reference proteome set) that also contained reversed versions for each of the entries and considering all of the SEQUEST peptides scores for the level of confidence of protein identification.[34] Identifications were filtered to two peptides per protein and 0% peptide false discovery rate and collated at the protein level using Scaffold (Proteome Software). Furthermore, MS/MS spectrum searches were performed with a tolerance of 2.5 Da (monoisotopic) and fragment ion tolerance of 0.5 Da (monoisotopic). Search criteria also included up to 10 missed cleavages, peptide threshold 95% (minimum), protein threshold 99.9% (minimum), and variable modifications, such as methionine (M) and histidine (H) oxidation and also (N-term) acetylation.

RESULTS AND DISCUSSION

Imaging Mass Spectrometry

IMS was used to assess spatial localization of proteins within focal areas of human pressure ulcer tissue sections. Currently, in the absence of validated tools, clinicians rely on subjective visual observations at the bedside to provide guidance. Our study included samples removed from stage IV pressure ulcers under various conditions ranging from stagnant, intractable sores to those showing nascent evidence of improvement. Attention was focused within three regions of interest: the wound bed, adjacent dermis, and hypertrophic epidermis at the wound's edge. Among the discovery data set, we discovered multiple proteins within a family of calcium-modulated proteins such as calcyclin (S100-A6), calgranulin A (S100-A8) and B (S100-A9), and calgizzarin (S100-A11), displaying uniquely different localizations in pressure ulcer samples under different healing conditions. The S100 proteins identified are uniquely expressed in vertebrates[35] and have been implicated to date in a variety of cellular activities including signal transduction, cell

dx.doi.org/10.1021/pr5010218 | J. Proteome Res. 2015, 14, 986–996

differentiation, regulation of cell motility, transcription and regeneration in mouse ear wounds.[35−37]

Figure 1 displays a series of two-dimensional ion density maps for human defensin 6 (HD-6), calcyclin, calgranulin A, calgizzarin, and calgranulin B. These ion density maps are plotted for three representative pressure ulcer samples from different patients (Table 1), highlighting chronically stagnant, unmistakable healing, and also intermediate or modest healing states. In our earlier publication, we documented that several members of the human defensin family (HNP-1, -2, -3) were differentially expressed in the wound beds exhibiting little or no evidence of healing. In this article, we extend these findings to include the ion at m/z 3708, human defensin 6 (HD-6). This molecule was strictly localized to the wound bed in both the chronic, stagnant wound beds and in the intermediate (modestly healing) samples, whereas it was poorly expressed in the healing sample, where it showed no particular localization. This report extends our earlier impressions that defensins may serve as markers for wounds that are struggling to overcome the prevailing factors that are responsible for wound chronicity.

Table 1. Patient Demographics

patient	age	sex	race[a]
1	69	F	C
2	18	M	C
3	41	M	C
4	26	M	C
5	37	M	C
6	37	F	C
7	47	M	C
8	64	M	C
9	39	F	C
10	19	M	C
11	73	F	C
12	38	M	C
13	47	M	C
14	19	M	AA
15	42	F	AA

[a]C, Caucasian; AA, African American.

Figure 1 shows that calcyclin, the ion at m/z 10 093, was distributed into the adjacent dermis in the case of the chronic (nonhealing) sample as well as into the hypertrophic epidermis in the case of the healing sample. Furthermore, the same protein expression in the intermediate healing sample highlights a different localization in the papillary (upper) dermis, close to the wound bed. Recently, calcyclin has been associated with the mechanism of promoting colorectal cancer metastasis[38] and, when underexpressed, with small cell lung cancer,[39,40] but it has little or no prior association with the events of wound healing.

Two other calcium binding proteins, calgranulin A and B, respectively at m/z 10 834 and 13 150, displayed a unique localization pattern within the pressure ulcers regions. Both proteins were restricted to the wound bed in the chronic (nonhealing) condition, but in the samples with robust healing, they were localized only in the hypertrophic epidermis close to the wound bed. The intermediate healing condition displayed these proteins in both the hypertrophic epidermis and throughout the wound bed. Thus, these two calcium-dependent molecules show a dynamic modulation, providing indirect clues that they play a heretofore undefined role in injury and repair. Often, calgranulin A and B, recently reviewed by Moore et al.,[41] are found to be aggregated into a complex known as calprotectin. This configuration has been shown to enhance neutrophil migration to inflammatory sites in a murine model and IMS has been used to detect heterodimer subunits of calprotectin as a marker of the inflammatory response to bacterial challenge.[42] Mounting evidence suggests that calgranulins function in anti-inflammatory and antimicrobial roles.[43] They have been identified in numerous inflammatory diseases, including rheumatoid arthritis, chronic periodontal disease, connective tissue disease, psoriasis, and bacterial pulmonary infection.[41,44−46] In addition, these proteins are involved in wound repair and reorganization of keratinocyte resistance to bacteria[43] and are increased following epidermal injury.[36,47] Eming et al. have reported elevated calgranulin B in wound exudates.[48] Our discovery of calgranulin A and B in chronic wound tissues should provide additional impetus to examine the role of calcium-dependent reactions during the

Table 2. Localization of Proteins of Note within Each Patient Sample[a]

patient	human defensin-6 m/z 3708	thymosin beta-10 m/z 4736	thymosin beta-4 trunc. m/z 4748	calcyclin m/z 10 093	calgranulin A m/z 10 834	calgizzarin m/z 11 656	calgranulin B m/z 13 150
1	W	D	D	D	W, E	D, E	W, E
2	W	D	D	D	E	D, E	E
3	W	NL	D	D	NL	D, lower W	W
4	W	NL	NL	D	W	D	W
5	W, low	D	D	NL	E	E	E
6	W, low	D	D	D	W	D, W	W
7	D, low	E, low	E, low	E	NL	E	E, low
8	W, low	D	D	D	W	E	E
9	NL	D	D, restricted	E	E	E	E
10	NL	D, E	D	D	E	D, E	E
11	W	D, W	D, W	D	W, E	D, upper	E
12	NL	NL	NL	D, E	E	E	E
13	W	D, E	D, E	NL	D, upper	E	E
14	W	lower D	lower D	D, E	W, E	E	E
15	W	D, low	D, low	D	W, E, D upper	D, E	E

[a]W, wound bed; D, adjacent dermis; E, hypertrophic epidermis; and NL, not localized (undetectable). A distribution restricted to the upper dermis (upper), lower dermis (lower). Low indicates a relatively low, but detectable level.

dx.doi.org/10.1021/pr5010218 | J. Proteome Res. 2015, 14, 986−996

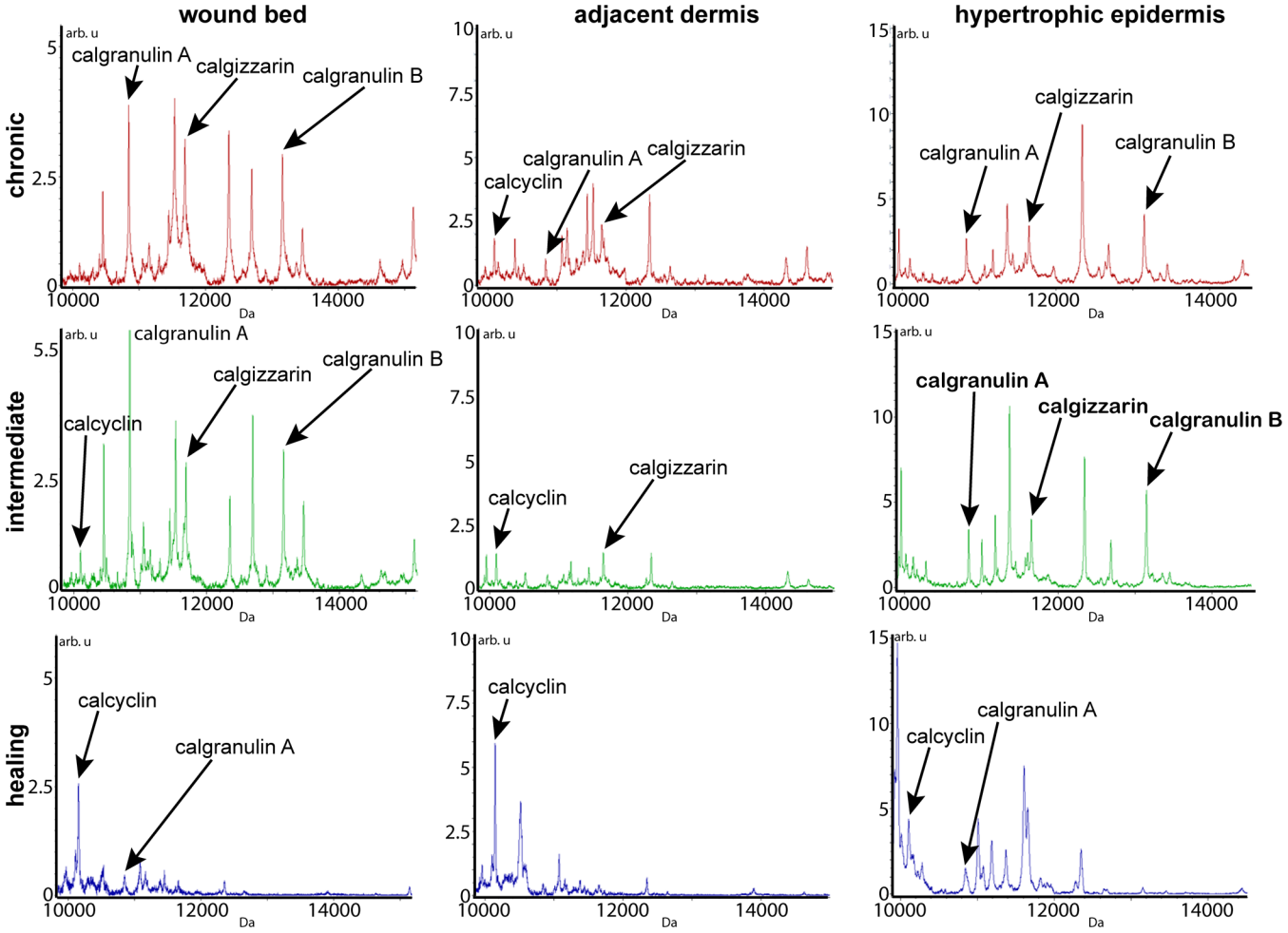

Figure 2. Averaged spectra from all of the samples included in the study. The *x* axis is truncated to show peaks for calcium binding molecules in the molecular weight range of 10−15 kDa. The *y* axis is expressed in arbitrary units but is held constant within each focal area (wound bed, adjacent dermis, hypertrophic epidermis). Each row reveals that each focal area has a unique footprint of spectral values.

reparative process. At a minimum, these data suggest that the presence of calgranulins A and B indicates a wound that is still largely characterized as being predominantly in the inflammatory phase.

Another member of the calcium binding family, the ion at *m*/*z* 11 656, calgizzarin, also displayed changes in localization among different healing conditions. The chronic, stagnant wound sample regionally displayed this protein in the wound bed but also throughout the adjacent dermis, similar to the calcyclin distribution. By contrast, the healing sample displayed calgizzarin with a relatively high expression into the hypertrophic epidermis, similar to the calgranulin A and B distributions. The intermediate healing state presented an unrestricted distribution throughout both the epidermis and the papillary dermis. The differential distribution pattern for calgizzarin within various stages and focal areas of interest was not surprising. Differential expression of calgizzarin has been previously reported and used to distinguish colorectal carcinoma from colon adenoma,[49] a setting where there is also rapid growth and transition of tissue morphology. These protein localization trends were consistently obvious in the other samples examined in this study (see Supporting Information Figure 1). Table 2 provides localization information for the calcium binding molecules of note with each of the 15 patient samples, as well as that of several nonmodulated constitutive proteins.

Spectral Profiling

Spectra highlighting the distribution of specific proteins within the regions of interest were exported from the imaging data sets from all of the samples using guidance from hematoxylin and eosin stained serial tissue sections, and the coordinates were provided by the ion density maps. Figure 2 shows the averaged spectra, normalized to the TIC, recorded from all of the chronic (stagnant), intermediate (modest or nascent) healing, and the firmly established healing samples. Spectra were plotted into the mass range 10−15 kDa, focusing on calcium binding proteins within that mass range. However, additional spectra were acquired in the mass range 3−30 kDa (see Supporting Information Figure 2). In general, all of the averaged spectra from chronic (stagnant) wound examples highlighted signals related to calcyclin, calgranulin A and B, and calgizzarin. Spectra profiled from the definitively healing wound examples instead displayed mainly calcyclin and calgranulin A. However, calgranulin A had a relatively low expression overall in these wounds. In summary, the averaged spectra from the chronic (stagnant) samples always displayed calcium binding protein signals, whereas the averaged spectra from the wounds in the healing phases displayed a predominant expression of calcyclin and a relatively low, yet specific, expression of calgranulin A.

dx.doi.org/10.1021/pr5010218 | J. Proteome Res. 2015, 14, 986−996

Table 3. A Selection of Protein IDs and the Corresponding Numbers of Peptides and Spectra

protein name	accession no.	molecular weight (Da)	no. of unique peptides		no. of assigned spectra	
			wound	adjcent dermis	wound	adjacent dermis
78 kDa glucose-regulated protein	P11021	72 335	4	3	4	3
Actin, aortic smooth muscle	P62736	4201	2	5	2	6
Actin, cytoplasmic 1	P60709	41 793	12	10	16	15
Alpha-1-antitrypsin	P01009	46 737	6	8	6	9
Alpha-2-macroglobulin	P01023	163 289	4	6	4	6
Alpha-actinin-4	O43707	104 857	0	4	0	4
Alpha-enolase	P06733	47 170	5	1	6	1
Annexin A1	P04083	38 715	2	3	3	3
Annexin A5	P08758	35 938	0	3	0	3
Annexin A6	P08133	75 877	3	3	3	3
Apolipoprotein A-I	P02647	30 778	2	4	2	4
Caldesmon	Q05682	61 706	3	3	3	3
Cofilin-1	P23528	18 503	3	0	4	0
Collagen alpha-1(I) chain	P02452	138 941	10	27	10	44
Collagen alpha-1(III) chain	P02461	13 856	6	15	6	21
Collagen alpha-1(VI) chain	P12109	108 531	1	4	1	6
Collagen alpha-1(XII) chain	Q99715	333 145	3	1	3	1
Collagen alpha-1(XIV) chain	Q05707	193 516	0	7	0	7
Collagen alpha-2(I) chain	P08123	129 315	10	25	10	32
Collagen alpha-2(VI) chain	P12110	108 581	2	9	2	12
Collagen alpha-3(VI) chain	P12111	343 667	6	28	8	34
Complement C3	P01024	187 149	7	10	8	13
Complement C4-A	P0C0L4	192 773	2	3	2	3
Desmin	P17661	53 537	0	4	0	4
Elastin	P15502	26 177	0	3	0	4
Elongation factor 1-alpha 1	P68104	50 141	0	3	0	3
Fibrinogen alpha chain	P02671	94 973	10	4	11	6
Fibrinogen beta chain	P02675	55 929	15	9	19	10
Fibrinogen gamma chain	P02679	51 513	8	6	11	8
Fibronectin	P02751	262 617	4	2	4	2
Filamin-A	P21333	280 729	1	4	1	4
Gelsolin	P06396	85 698	3	1	4	1
Glyceraldehyde-3-phosphate dehydrogenase	P04406	36 053	3	4	3	4
Haptoglobin	P00738	45 205	5	5	5	5
Heat shock 70 kDa protein 1A/1B	P08107	70 054	1	5	1	5
Heat shock protein HSP 90-alpha	P07900	84 663	1	3	1	4
Hemoglobin subunit alpha	P69905	15 258	5	3	7	4
Hemoglobin subunit beta	P68871	15 998	5	5	5	9
Heterogeneous nuclear ribonucleoprotein K	P61978	50 979	1	3	1	3
Histone H1.4	P10412	21 867	4	1	4	1
Histone H4	P62805	11 368	1	3	1	3
Human defensin alpha 6	Q01524	10 975	2	0	4	0
Ig alpha-1 chain C region	P01876	37 654	3	4	3	4
Ig gamma-1 chain C region	P01857	36 105	4	2	5	2
Ig gamma-2 chain C region	P01859	35 899	3	1	5	1
Ig kappa chain C region	P01834	11 609	3	3	3	4
keratin 1, type II, cytoskeletal	gi7428712	65 495	0	2	1	4
Lumican	P51884	38 432	0	5	0	5
Moesin	P26038	67 822	2	3	2	3
Myosin light polypeptide 6	P60660	17 089	3	2	3	2
Myosin-9	P35579	226 538	16	9	17	9
Neuroblast differentiation-associated protein	Q09666	629 104	1	9	1	9
Peptidyl-prolyl cis−trans isomerase A	P62937	18 013	0	4	0	4
Plasma protease C1 inhibitor	P05155	49 758	2	3	2	3
Plastin-2	P13796	70 291	7	2	7	2
Plectin	Q15149	531 784	0	3	0	3
Prelamin-A/C	P02545	74 141	1	6	1	7
Protein S100-A11, calgizzarin	P31949	11 740	2	3	4	2
Protein S100-A6, calcyclin	P06703	10 180	2	2	6	6

dx.doi.org/10.1021/pr5010218 | J. Proteome Res. 2015, 14, 986−996

Table 3. continued

protein name	accession no.	molecular weight (Da)	no. of unique peptides		no. of assigned spectra	
			wound	adjcent dermis	wound	adjacent dermis
Protein S100-A8, calgranulin A	P05109	10 835	3	2	6	2
Protein S100-A9, calgranulin B	P06702	13 242	3	2	5	2
Pyruvate kinase isozymes M1/M2	P14618	57 938	3	4	3	4
Serum albumin	P02768	69 367	13	15	17	23
Talin-1	Q9Y490	269 765	4	1	4	1
Transgelin	Q01995	22 611	3	4	3	4
Tropomyosin alpha-4 chain	P67936	28 522	0	3	0	3
Tubulin alpha-1B chain	P68363	46 298	2	4	3	4
Tubulin beta chain	P07437	48 461	4	0	4	0
Vimentin	P08670	53 653	13	13	14	13
Vitronectin	P04004	54 306	1	3	1	3

Interestingly, spectra for calgranulin A display a similar pattern as that of HD-6, as both molecules are present in chronic (stagnant) wound beds but not in those that were well on their way toward healing. In addition, calgranulin A is not detectable in the adjacent dermis of intermediate and healing wounds. Calgranulin A appeared to be restricted to the hypertrophic epidermis of the healing wounds (see Supporting Information Figure 3). Spectra recorded from wounds in the intermediate healing condition displayed a protein pattern similar to that of the chronic state but with different relative expression levels. Interestingly, the signal representing calcyclin was not detected in the spectra averaged from the chronic (stagnant) wound beds but was present in both the intermediate and healing wound beds.

Table 3 provides a listing of identified proteins with the corresponding accession numbers, molecular weight, and number of assigned spectra and unique identified peptides from different skin tissue regions, wound bed and adjacent dermis. Table 4, instead, provides a listing of identified proteins from wounds with a chronic or healing status and displays whether they were detected in the wound bed, adjacent dermis, or both. Interestingly, many proteins on this list are uniquely identified within chronic (stagnant) wounds, and the majority of those are isolated to a specific region of interest. While our report predominantly highlights the theme of calcium-modulating proteins, our discovery approach indicates a much broader, rich field of molecules for future exploration. All of the information related to the level of confidence of the protein identification, such as protein identification probability, percentage of sequence coverage, peptide sequences, and related scores, are reported as Supporting Information (Tables 1 and 2).

Principal Component Analysis

Imaging data sets were also subjected to principal component analysis (PCA) to validate the changes in protein patterns/trends within different healing conditions. Figure 3a displays three PCA plots, where spectra from each region of interest were compared to each other in the three healing conditions. These statistical approaches generated distinct spectra clusters based on condition or region within the cohort. In the case of chronic (stagnant) samples, spectra clusters from wound bed, adjacent dermis, and hypertrophic epidermis were widely separated from each other. In the samples displaying morphological and clinical evidence of robust healing, spectra clusters from the wound bed and the adjacent dermis areas overlapped, whereas spectra from the hypertrophic epidermis clustered separately. This latter finding suggests that in circumstance of robust and definitive healing the protein patterns from the two neighboring tissue areas (wound bed and the adjacent dermis) are more similar than those in the circumstance of chronic, stagnant wounds, where the wound regions highlighted a different protein pattern. Furthermore, spectra sets from the hypertrophic epidermis always displayed separately within the PCA plots regardless of healing condition. This was expected since epidermis and dermis consist of entirely different cell populations and thus serve as an internal validation tool of our processes. Samples showing evidence of healing in the intermediate phases, similar to the samples displaying chronic (stagnant) wounds, showed all three regional spectra clusters differentially distributed within the PCA plot, although in this group the three unique clusters plotted closer to each other than in the chronic condition.

Figure 3b displays a different representation of the same data in three additional PCA plots: comparing spectra data sets from different healing conditions (chronic, intermediate, and healing) within the regions of interest. Wound bed spectra sets were clustered and separated within the PCA plot with some overlap between chronic and intermediate wound beds, whereas spectra from healing wound beds clustered separately. In the case of hypertrophic epidermis and adjacent dermis, both the chronic and the intermediate spectra clusters, although close, were distinctly different in distribution, whereas the spectra from the healing samples continued to show a more varied distribution.

■ CONCLUSIONS

Imaging mass spectrometry can provide swift information on both the distribution and relative amounts of biocompounds within a thin tissue section.[7,10,50−52] In our study, IMS uncovered differential protein distributions in three different tissue niches within pressure wounds. This demonstrated that this technique can yield new clues with relative expression and spatial localization that have not been previously identified through traditional histology staining or analysis of wound fluids. Cell and tissue specific molecular profiles and images in correlation with tradition histology show promise as diagnostic tools of higher specificity and sensitivity to complement classical visual approaches by clinicians.

In this study, our attention was focused on a set of calcium binding proteins from the S100 family and their distribution and localization within pressure ulcer wound beds and adjacent areas. Such proteins are usually expressed by circulating neutrophils and monocytes representing the first cells to

Table 4. Locations of Identified Proteins

protein name	accession no.	chronic	healing	both	wound bed	adjacent dermis	both
78 kDa glucose-regulated protein	P11021	×					×
Actin, aortic smooth muscle	P62736	×				×	
Actin, cytoplasmic 1	P60709			×			×
Alpha-1-antitrypsin	P01009			×			×
Alpha-2-macroglobulin	P01023			×			×
Alpha-actinin-4	O43707	×				×	
Alpha-enolase	P06733			×	×		
Annexin A1	P04083	×				×	
Annexin A5	P08758	×				×	
Annexin A6	P08133	×					×
Apolipoprotein A-I	P02647		×			×	
Caldesmon	Q05682	×					×
Cofilin-1	P23528			×	×		
Collagen alpha-1(I) chain	P02452			×			×
Collagen alpha-1(III) chain	P02461			×			×
Collagen alpha-1(VI) chain	P12109			×		×	
Collagen alpha-1(XII) chain	Q99715	×			×		
Collagen alpha-1(XIV) chain	Q05707			×		×	
Collagen alpha-2(I) chain	P08123		×				×
Collagen alpha-2(VI) chain	P12110			×		×	
Collagen alpha-3(VI) chain	P12111			×			×
Complement C3	P01024			×			×
Complement C4-A	P0C0L4	×				×	
Desmin	P17661	×				×	
Elastin	P15502			×		×	
Elongation factor 1-alpha 1	P68104	×				×	
Fibrinogen alpha chain	P02671			×			×
Fibrinogen beta chain	P02675			×			×
Fibrinogen gamma chain	P02679			×			×
Fibronectin	P02751			×	×		
Filamin-A	P21333	×				×	
Gelsolin	P06396			×	×		
Glyceraldehyde-3-phosphate dehydrogenase	P04406			×			×
Haptoglobin	P00738			×			×
Heat shock 70 kDa protein 1A/1B	P08107	×				×	
Heat shock protein HSP 90-alpha	P07900	×				×	
Hemoglobin subunit alpha	P69905			×			×
Hemoglobin subunit beta	P68871			×			×
Heterogeneous nuclear ribonucleoprotein K	P61978	×					×
Histone H1.4	P10412	×			×		
Histone H4	P62805	×				×	
Human defensin alpha 6	Q01524	×			×		
Ig alpha-1 chain C region	P01876			×			×
Ig gamma-1 chain C region	P01857			×	×		
Ig gamma-2 chain C region	P01859			×	×		
Ig kappa chain C region	P01834			×			×
keratin 1, type II, cytoskeletal	gi7428712			×		×	
Lumican	P51884			×		×	
Moesin	P26038			×		×	
Myosin light polypeptide 6	P60660	×			×		
Myosin-9	P35579	×					×
Neuroblast differentiation-associated protein	Q09666	×				×	
Peptidyl-prolyl cis−trans isomerase A	P62937			×		×	
Plasma protease C1 inhibitor	P05155	×				×	
Plastin-2	P13796			×	×		
Plectin	Q15149	×				×	
Prelamin-A/C	P02545	×				×	
Protein S100-A11, calgizzarin	P31949			×		×	
Protein S100-A6, calcyclin	P06703			×			×
Protein S100-A8, calgranulin A	P05109			×	×		
Protein S100-A9, calgranulin B	P06702			×	×		

dx.doi.org/10.1021/pr5010218 | J. Proteome Res. 2015, 14, 986−996

Table 4. continued

protein name	accession no.	chronic	healing	both	wound bed	adjacent dermis	both
Pyruvate kinase isozymes M1/M2	P14618			×			×
Serum albumin	P02768			×			×
Talin-1	Q9Y490	×			×		
Transgelin	Q01995		×				×
Tropomyosin alpha-4 chain	P67936			×		×	
Tubulin alpha-1B chain	P68363	×				×	
Tubulin beta chain	P07437	×			×		
Vimentin	P08670			×			×
Vitronectin	P04004			×		×	

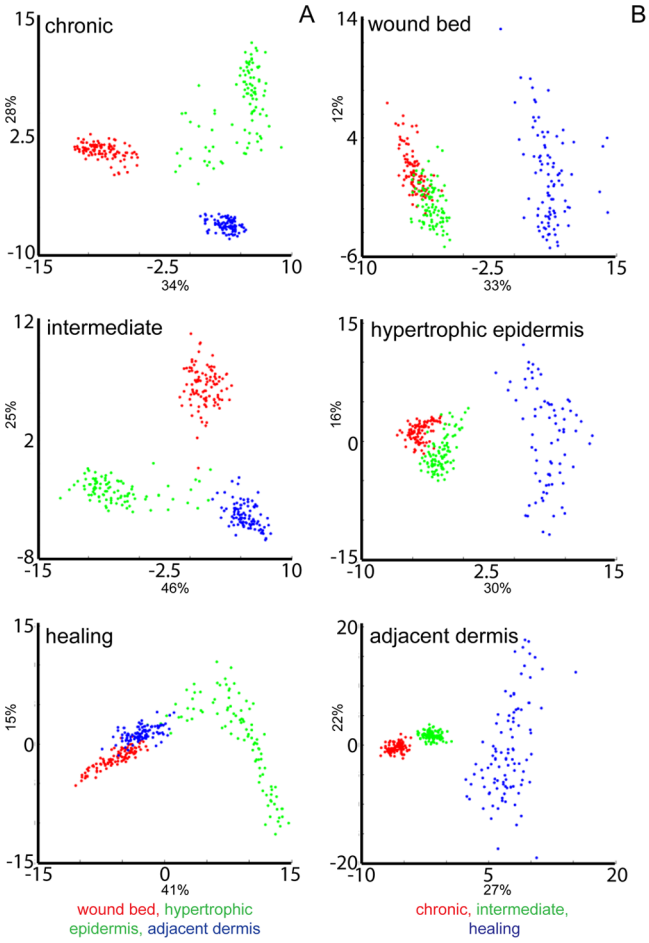

Figure 3. Principal component analysis data depicting the bulk of the proteins that were detected by IMS in the 3−30 kDa range. All of the pressure ulcers are included: chronic (stagnant) wounds, wounds with an intermediate (modest) improvement in healing, and wounds that exhibits excellent healing progression. Focal areas of interest include the wound bed and the adjacent dermis with its overlying hypertrophic epidermis.

invade inflammatory lesions.[53−55] In particular, calgranulin A and B have a cytotoxic effect that may play a role in several inflammatory diseases which are associated with endothelial dysfunction and pathologic accumulation of such proteins.[56] Furthermore, it was reported that S100 A8 and A9 form a hetero-oligomer called calprotectin, which plays a prominent role in the regulation of inflammatory processes and immune response.[57,58] Finally, this protein was recently also recognized as a novel player in wound repair after skin injury.[47]

In summary, the molecular signatures within the pressure ulcer appear to change dynamically in response to environmental pressures and subsequent signaling, all of which are events that are still poorly characterized. We have elucidated a pattern of calcium binding proteins within the pressure ulcer model that can potentially be used for healing prediction and possible mitigation of unfavorable outcomes.

■ ASSOCIATED CONTENT

Supporting Information

Figure 1: Ion-density maps from three additional pressure ulcer wounds. Figure 2: A series of averaged and TIC-normalized MALDI MS spectra highlighting the peaks in the molecular weight range of 4−20 kDa. Figure 3: A series of averaged and TIC-normalized MALDI MS spectra highlighting single peaks for human defensin 6 and calgranulin A from different tissue regions and at the opposite end of the healing continuum (stagnant, chronic wounds, and healing wounds). Table 1: Peptide coverage and confidence details for protein IDs in the wound. Table 2: Peptide coverage and confidence details for protein IDs in the adjacent dermis. This material is available free of charge via the Internet at http://pubs.acs.org.

■ AUTHOR INFORMATION

Corresponding Author

*E-mail: lillian.nanney@vanderbilt.edu. Phone: 615-322-7265.

Notes

The authors declare no competing financial interest.

(D.T.) Phone: +39 0984 493334; E-mail: domenico.taverna@unical.it. (A.C.P.) Phone: 615-322-7266; E-mail: alonda.c.pollins@vanderbilt.edu. (G.S.) Phone: +39 0984 492083; E-mail: giovanni.sindona@unical.it. (R.M.C.) Phone: 615-343-2700; richard.caprioli@vanderbilt.edu.

■ ACKNOWLEDGMENTS

This work was supported by the Commission European Union, European Social Funds (POR Calabria FSE 2007/2013) and the Region of Calabria (Taverna), NIH/NIAMS AR056138-01A2 (L.B.N.), and NIH/NIGMS 5P41 GM 103391-03 (R.M.C.). The authors thank W. Hayes McDonald at the Vanderbilt Proteomics Core Facility for LC−MS/MS support.

■ REFERENCES

(1) Di Donna, L.; Taverna, D.; Mazzotti, F. Comprehensive assay of flavanones in citrus juices and beverages by UHPLC-ESI-MS/MS and derivatization chemistry. *Food Chem.* **2013**, *141*, 2328−2333.

(2) Donna, L. D.; Mazzotti, F.; Taverna, D.; Napoli, A.; Sindona, G. Structural characterisation of malonyl flavonols in leek (*Allium porrum*

L.) using high-performance liquid chromatography and mass spectrometry. *Phytochem. Anal.* **2014**, *25*, 207−212.
(3) Mazzotti, F.; Di Donna, L.; Taverna, D.; et al. Evaluation of dialdehydic anti-inflammatory active principles in extra-virgin olive oil by reactive paper spray mass spectrometry. *Int. J. Mass Spectrom.* **2013**, *352*, 87−91.
(4) Taverna, D.; Di Donna, L.; Mazzotti, F.; Policicchio, B.; Sindona, G. High-throughput determination of Sudan Azo-dyes within powdered chili pepper by paper spray mass spectrometry. *J. Mass Spectrom.* **2013**, *48*, 544−547.
(5) Caprioli, R. M.; Farmer, T. B.; Gile, J. Molecular imaging of biological samples: localization of peptides and proteins using MALDI-TOF MS. *Anal. Chem.* **1997**, *69*, 4751−4760.
(6) Seeley, E. H.; Schwamborn, K.; Caprioli, R. M. Imaging of intact tissue sections: moving beyond the microscope. *J. Biol. Chem.* **2011**, *286*, 25459−25466.
(7) Seeley, E. H.; Caprioli, R. M. Molecular imaging of proteins in tissues by mass spectrometry. *Proc. Natl. Acad. Sci. U.S.A.* **2008**, *105*, 18126−18131.
(8) Schwartz, S. A.; Caprioli, R. M. Imaging mass spectrometry: viewing the future. *Methods Mol. Biol.* **2010**, *656*, 3−19.
(9) Vickerman, J. C. Molecular imaging and depth profiling by mass spectrometry—SIMS, MALDI or DESI? *Analyst* **2011**, *136*, 2199−2217.
(10) McDonnell, L. A.; Heeren, R. M. Imaging mass spectrometry. *Mass Spectrom. Rev.* **2007**, *26*, 606−643.
(11) Andersson, M.; Groseclose, M. R.; Deutch, A. Y.; Caprioli, R. M. Imaging mass spectrometry of proteins and peptides: 3D volume reconstruction. *Nat. Methods* **2008**, *5*, 101−108.
(12) Burnum, K. E.; Tranguch, S.; Mi, D.; Daikoku, T.; Dey, S. K.; Caprioli, R. M. Imaging mass spectrometry reveals unique protein profiles during embryo implantation. *Endocrinology.* **2008**, *149*, 3274−3278.
(13) Cazares, L. H.; Troyer, D.; Mendrinos, S. Imaging mass spectrometry of a specific fragment of mitogen-activated protein kinase/extracellular signal-regulated kinase kinase kinase 2 discriminates cancer from uninvolved prostate tissue. *Clin. Cancer Res.* **2009**, *15*, 5541−5551.
(14) Groseclose, M. R.; Andersson, M.; Hardesty, W. M.; Caprioli, R. M. Identification of proteins directly from tissue: in situ tryptic digestions coupled with imaging mass spectrometry. *J. Mass Spectrom.* **2007**, *42*, 254−262.
(15) Groseclose, M. R.; Massion, P. P.; Chaurand, P.; Caprioli, R. M. High-throughput proteomic analysis of formalin-fixed paraffin-embedded tissue microarrays using MALDI imaging mass spectrometry. *Proteomics.* **2008**, *8*, 3715−3724.
(16) Lemaire, R.; Desmons, A.; Tabet, J. C.; Day, R.; Salzet, M.; Fournier, I. Direct analysis and MALDI imaging of formalin-fixed, paraffin-embedded tissue sections. *J. Proteome Res.* **2007**, *6*, 1295−1305.
(17) Stoeckli, M.; Knochenmuss, R.; McCombie, G. MALDI MS imaging of amyloid. *Methods Enzymol.* **2006**, *412*, 94−106.
(18) Burnum, K. E.; Cornett, D. S.; Puolitaival, S. M. Spatial and temporal alterations of phospholipids determined by mass spectrometry during mouse embryo implantation. *J. Lipid Res.* **2009**, *50*, 2290−2298.
(19) Meriaux, C.; Franck, J.; Wisztorski, M.; Salzet, M.; Fournier, I. Liquid ionic matrixes for MALDI mass spectrometry imaging of lipids. *J. Proteomics.* **2010**, *73*, 1204−1218.
(20) Puolitaival, S. M.; Burnum, K. E.; Cornett, D. S.; Caprioli, R. M. Solvent-free matrix dry-coating for MALDI imaging of phospholipids. *J. Am. Soc. Mass Spectrom.* **2008**, *19*, 882−886.
(21) Khatib-Shahidi, S.; Andersson, M.; Herman, J. L.; Gillespie, T. A.; Caprioli, R. M. Direct molecular analysis of whole-body animal tissue sections by imaging MALDI mass spectrometry. *Anal. Chem.* **2006**, *78*, 6448−6456.
(22) Reyzer, M. L.; Hsieh, Y.; Ng, K.; Korfmacher, W. A.; Caprioli, R. M. Direct analysis of drug candidates in tissue by matrix-assisted laser desorption/ionization mass spectrometry. *J. Mass Spectrom.* **2003**, *38*, 1081−1092.
(23) Kim, Y.; Hurst, G. B.; Doktycz, M. J.; Buchanan, M. V. Improving spot homogeneity by using polymer substrates in matrix-assisted laser desorption/ionization mass spectrometry of oligonucleotides. *Anal. Chem.* **2001**, *73*, 2617−2624.
(24) *NPUAP Pressure Ulcer Stages*; National Pressure Ulcer Advisory Panel: Washington, DC, 2013; http://www.npuap.org/resources/educational-and-clinical-resources/npuap-pressure-ulcer-stagescategories/.
(25) Spear, M. Pressure ulcer staging-revisited. *Plast. Surg. Nurs.* **2013**, *33*, 192−194.
(26) Fogerty, M.; Guy, J.; Barbul, A.; Nanney, L. B.; Abumrad, N. N. African Americans show increased risk for pressure ulcers: a retrospective analysis of acute care hospitals in America. *Wound Repair Regener.* **2009**, *17*, 678−684.
(27) Fogerty, M. D.; Abumrad, N. N.; Nanney, L.; Arbogast, P. G.; Poulose, B.; Barbul, A. Risk factors for pressure ulcers in acute care hospitals. *Wound Repair Regener.* **2008**, *16*, 11−18.
(28) Sen, C. K.; Gordillo, G. M.; Roy, S. Human skin wounds: a major and snowballing threat to public health and the economy. *Wound Repair Regener.* **2009**, *17*, 763−771.
(29) Edsberg, L. E.; Wyffels, J. T.; Brogan, M. S.; Fries, K. M. Analysis of the proteomic profile of chronic pressure ulcers. *Wound Repair Regener.* **2012**, *20*, 378−401.
(30) Taverna, D.; Nanney, L. B.; Pollins, A. C.; Sindona, G.; Caprioli, R. Multiplexed molecular descriptors of pressure ulcers defined by imaging mass spectrometry. *Wound Repair Regener.* **2011**, *19*, 734−744.
(31) Taverna, D.; Nanney, L. B.; Pollins, A. C.; Sindona, G.; Caprioli, R. Spatial mapping by imaging mass spectrometry offers advancements for rapid definition of human skin proteomic signatures. *Exp. Dermatol.* **2011**, *20*, 642−647.
(32) Harris, G. A.; Nicklay, J. J.; Caprioli, R. M. Localized in situ hydrogel-mediated protein digestion and extraction technique for on-tissue analysis. *Anal. Chem.* **2013**, *85*, 2717−2723.
(33) Nicklay, J. J.; Harris, G. A.; Schey, K. L.; Caprioli, R. M. MALDI Imaging and in situ identification of integral membrane proteins from rat brain tissue sections. *Anal. Chem.* **2013**, *85*, 7191−7196.
(34) Yates, J. R.; Eng, J. K.; McCormack, A. L.; Schieltz, D. Method to correlate tandem mass spectra of modified peptides to amino acid sequences in the protein database. *Anal. Chem.* **1995**, *67*, 1426−1436.
(35) Heizmann, C. W.; Ackermann, G. E.; Galichet, A. Pathologies involving the S100 proteins and RAGE. *Subcell. Biochem.* **2007**, *45*, 93−138.
(36) Eckert, R. L.; Broome, A. M.; Ruse, M.; Robinson, N.; Ryan, D.; Lee, K. S100 proteins in the epidermis. *J. Invest. Dermatol.* **2004**, *123*, 23−33.
(37) Caldwell, R. L.; Opalenik, S. R.; Davidson, J. M.; Caprioli, R. M.; Nanney, L. B. Tissue profiling MALDI mass spectrometry reveals prominent calcium-binding proteins in the proteome of regenerative MRL mouse wounds. *Wound Repair Regener.* **2008**, *16*, 442−449.
(38) Ghosh, D.; Li, Z.; Tan, X. F.; Lim, T. K.; Mao, Y.; Lin, Q. iTRAQ based quantitative proteomics approach validated the role of calcyclin binding protein (CacyBP) in promoting colorectal cancer metastasis. *Mol. Cell. Proteomics* **2013**, *12*, 1865−1880.
(39) Lee, H. S.; Park, J. W.; Chertov, O. Matrix-assisted laser desorption/ionization mass spectrometry reveals decreased calcylcin expression in small cell lung cancer. *Pathol. Int.* **2012**, *62*, 28−35.
(40) Jiang, H.; Hu, H.; Tong, X.; Jiang, Q.; Zhu, H.; Zhang, S. Calcium-binding protein S100P and cancer: mechanisms and clinical relevance. *J. Cancer Res. Clin. Oncol.* **2012**, *138*, 1−9.
(41) Moore, J. L.; Becker, K. W.; Nicklay, J. J.; Boyd, K. L.; Skaar, E. P.; Caprioli, R. M. Imaging mass spectrometry for assessing temporal proteomics: analysis of calprotectin in *Acinetobacter baumannii* pulmonary infection. *Proteomics* **2013**, *14*, 820−828.
(42) Ryckman, C.; Vandal, K.; Rouleau, P.; Talbot, M.; Tessier, P. A. Proinflammatory activities of S100: proteins S100A8, S100A9, and

S100A8/A9 induce neutrophil chemotaxis and adhesion. *J. Immunol.* **2003**, *170*, 3233−3242.
(43) Hsu, K.; Champaiboon, C.; Guenther, B. D. Anti-infective protective properties of S100 calgranulins. *Anti-Inflammatory Anti-Allergy Agents Med. Chem.* **2009**, *8*, 290−305.
(44) Foell, D.; Kane, D.; Bresnihan, B. Expression of the pro-inflammatory protein S100A12 (EN-RAGE) in rheumatoid and psoriatic arthritis. *Rheumatology* **2003**, *42*, 1383−1389.
(45) Leach, S. T.; Yang, Z.; Messina, I. Serum and mucosal S100 proteins, calprotectin (S100A8/S100A9) and S100A12, are elevated at diagnosis in children with inflammatory bowel disease. *Scand. J. Gastroenterol.* **2007**, *42*, 1321−1331.
(46) Striz, I.; Trebichavsky, I. Calprotectin—a pleiotropic molecule in acute and chronic inflammation. *Physiol. Res.* **2004**, *53*, 245−253.
(47) Thorey, I. S.; Roth, J.; Regenbogen, J. The Ca^{2+}-binding proteins S100A8 and S100A9 are encoded by novel injury-regulated genes. *J. Biol. Chem.* **2001**, *276*, 35818−35825.
(48) Eming, S. A.; Koch, M.; Krieger, A. Differential proteomic analysis distinguishes tissue repair biomarker signatures in wound exudates obtained from normal healing and chronic wounds. *J. Proteome Res.* **2010**, *9*, 4758−4766.
(49) Melle, C.; Ernst, G.; Schimmel, B. Different expression of calgizzarin (S100A11) in normal colonic epithelium, adenoma and colorectal carcinoma. *Int. J. Oncol.* **2006**, *28*, 195−200.
(50) Amstalden van Hove, E. R.; Smith, D. F.; Heeren, R. M. A concise review of mass spectrometry imaging. *J. Chromatogr. A* **2010**, *1217*, 3946−3954.
(51) Cornett, D. S.; Reyzer, M. L.; Chaurand, P.; Caprioli, R. M. MALDI imaging mass spectrometry: molecular snapshots of biochemical systems. *Nat. Methods* **2007**, *4*, 828−833.
(52) Pacholski, M. L.; Winograd, N. Imaging with mass spectrometry. *Chem. Rev.* **1999**, *99*, 2977−3006.
(53) Edgeworth, J.; Gorman, M.; Bennett, R.; Freemont, P.; Hogg, N. Identification of p8,14 as a highly abundant heterodimeric calcium binding protein complex of myeloid cells. *J. Biol. Chem.* **1991**, *266*, 7706−7713.
(54) Roth, J.; Burwinkel, F.; van den Bos, C.; Goebeler, M.; Vollmer, E.; Sorg, C. MRP8 and MRP14, S-100-like proteins associated with myeloid differentiation, are translocated to plasma membrane and intermediate filaments in a calcium-dependent manner. *Blood* **1993**, *82*, 1875−1883.
(55) Zwadlo, G.; Bruggen, J.; Gerhards, G.; Schlegel, R.; Sorg, C. Two calcium-binding proteins associated with specific stages of myeloid cell differentiation are expressed by subsets of macrophages in inflammatory tissues. *Clin. Exp. Immunol.* **1988**, *72*, 510−515.
(56) Viemann, D.; Barczyk, K.; Vogl, T. MRP8/MRP14 impairs endothelial integrity and induces a caspase-dependent and -independent cell death program. *Blood* **2007**, *109*, 2453−2460.
(57) Korndorfer, I. P.; Brueckner, F.; Skerra, A. The crystal structure of the human (S100A8/S100A9)2 heterotetramer, calprotectin, illustrates how conformational changes of interacting alpha-helices can determine specific association of two EF-hand proteins. *J. Mol. Biol.* **2007**, *370*, 887−898.
(58) Steinbakk, M.; Naess-Andresen, C. F.; Lingaas, E.; Dale, I.; Brandtzaeg, P.; Fagerhol, M. K. Antimicrobial actions of calcium binding leucocyte L1 protein, calprotectin. *Lancet* **1990**, *336*, 763−765.